NANO LETTERS

Letter

pubs.acs.org/NanoLett

Broken Symmetry Quantum Hall States in Dual-Gated ABA Trilayer Graphene

Yongjin Lee,[†] Jairo Velasco, Jr,[†] David Tran,[†] Fan Zhang,[‡] W. Bao,[†] Lei Jing,[†] Kevin Myhro,[†] Dmitry Smirnov,[§] and Chun Ning Lau*,[†]

[†]Department of Physics and Astronomy, University of California, Riverside, Riverside, California 92521, United States

[‡]Department of Physics and Astronomy, University of Pennsylvania, Philadelphia, Pennsylvania 19104, United States

[§]National High Magnetic Field Laboratory, Tallahassee, Florida 32310, United States

ABSTRACT: ABA-stacked trilayer graphene is a unique 2D electron system with mirror reflection symmetry and unconventional quantum Hall effect. We present low-temperature transport measurements on dual-gated suspended trilayer graphene in the quantum Hall (QH) regime. We observe QH plateaus at filling factors $\nu = -8, -2, 2, 6$, and 10, which is in agreement with the full-parameter tight binding calculations. In high magnetic fields, odd-integer plateaus are also resolved, indicating almost complete lifting of the 12-fold degeneracy of the lowest Landau level (LL). Under an out-of-plane electric field $E_\perp$, we observe degeneracy breaking and transitions between QH plateaus. Interestingly, depending on its direction, $E_\perp$ selectively breaks the LL degeneracies in the electron-doped or hole-doped regimes. Our results underscore the rich interaction-induced phenomena in trilayer graphene.

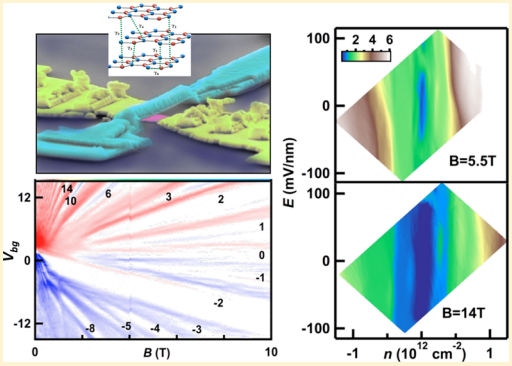

KEYWORDS: *Trilayer graphene, quantum Hall effect, broken symmetries, Landau level crossing*

As a fascinating two-dimensional (2D) system with chiral charge carriers and spectacular electronic, mechanical and thermal properties, graphene, and its multilayer counterparts[1−3] have emerged as new platforms for investigation of quantum Hall (QH) physics. A number of novel phenomena have been observed, such as multicomponent fractional QH effect in monolayer graphene (MLG),[4−7] insulating $\nu = 0$ states in MLG and bilayer graphene (BLG),[8−17] electric field-driven transitions among symmetry-broken QH states in BLG,[14,15] and chiral charge carriers with berry phase of 3π[18] and Lifshitz transition in ABC-stacked trilayer graphene (TLG).[19]

Like MLG and BLG, TLG offers an exciting platform with unique band structures. In particular, ABA-stacked TLG hosts mirror symmetry with respect to the middle layer (Figure 1a inset), and its band structure can be viewed as a combination of the linear dispersion of MLG and parabolic dispersion of BLG, that is, the so-called "2 + 1" model within tight-binding calculations[20−28] (Figure 1a,b). Though TLG has attracted more attention recently,[18,19,29−35] the nature of broken symmetry QH states in TLG and their evolutions under electric and magnetic fields remain experimentally unexplored.

In this Letter, we report transport measurements on high mobility dual-gated ABA TLG devices in the QH regime. At low magnetic field $B < 4$T, we resolve single particle QH states at filling factors $\nu = -8, -2, 2, 6$, and 10, which can be accounted for by the "2 + 1" tight-binding model that includes all hopping parameters.[36] At higher B, we observe additional states at $\nu = \pm1, \pm3, -4$, and -5, indicating almost complete lifting of the degeneracy of the lowest Landau level (LL). At constant B, application of an out-of-plane electric field $E_\perp$ gives rise to degeneracy breaking and transitions between QH plateaus, suggesting the interplay of layer polarization induced

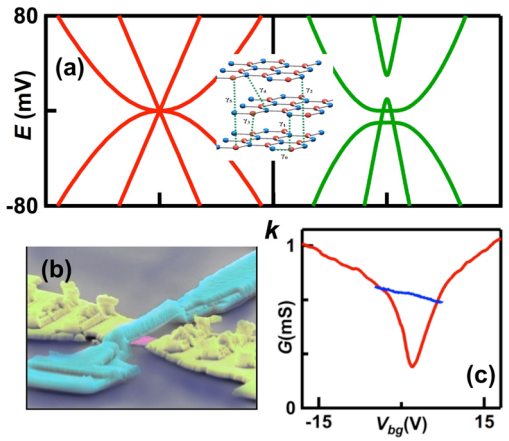

Figure 1. (a). Low-energy band structure of ABA-stacked TLG calculating (left panel) using only γ_0 and γ_1, (right panel) using γ_0−γ_5. Inset: ABA-stacked TLG lattice with hopping parameters γ_1−γ_5. (b). SEM image of a dual-gated suspended TLG device. (c) $G(V_{bg})$ before (blue) and after (red) current annealing.

Received: January 8, 2013
Revised: March 23, 2013

 © XXXX American Chemical Society dx.doi.org/10.1021/nl4000757 | *Nano Lett.* XXXX, XXX, XXX−XXX

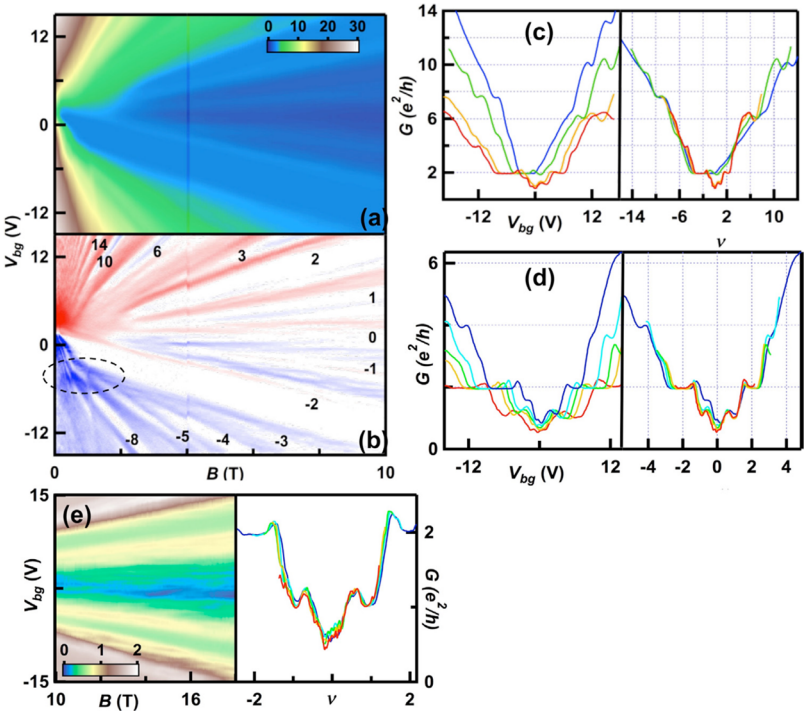

Figure 2. (a,b) $G(V_{bg}, B)$ and dG/dV_{bg} of a TLG device. Numbers indicate filling factors. The color scale in a indicates conductance in units of $e^2/\hbar$. (c). $G(V_{bg})$ and $G(\nu)$ at B = 1.5, 2.2, 3.5, and 4.2 T, respectively (from blue to red). (d). $G(V_{bg})$ and $G(\nu)$ at B = 4.5, 6, 7, 8, and 10 T (from blue to red). (e). $G(V_{bg}, B)$ and $G(\nu)$ at B = 10, 12, 14, 16 and 18 T (from blue to red).

by $E_\perp$ and B-enhanced exchange interactions of these states. Finally, depending on its polarity, we find the $E_\perp$ selectively breaks the LL degeneracy in the electron-doped or hole-doped regimes.

TLG sheets are isolated via mechanical exfoliation on Si/SiO_2 substrates, identified by optical contrast and Raman spectroscopy,[37] and coupled to Cr/Au electrodes and Cr suspended top gates.[38,39] The stacking order is ascertained by Raman spectroscopy,[40] the very strong $\nu = -2$ quantum Hall plateau[33] and absence of Lifshitz transition.[19] The devices are completed by removal of SiO_2 under the graphene with HF etching (Figure 1b). A typical device has source−drain separation 1.3 μm, and width 1.4−1.6 μm. All data are taken at 300 mK in He^3 refrigerators, and similar phenomena are observed in three devices.

An important advantage of the suspended top-gate structure is its compatibility with postfabrication annealing that may dramatically improve sample quality. Figure 1c displays the two-terminal conductance G as a function of back gate V_{bg} before (blue curve) and after (red curve) current annealing. After annealing, the curve becomes "V"-shaped, with charge neutrality close to zero, drastically lower minimum conductance, and high field effect mobility of ~15 000 $cm^2/(V\,s)$. We note that the typical contact resistance of our two-terminal device is less than 200 Ω, which can be ascertained from the deviation of the QH plateaus from their expected values.

In the simplest tight binding model that includes only the nearest neighbor in-plane and interplane hopping parameters γ_0 and γ_1, the band structure of ABA-stacked TLG consists of the MLG-like and BLG-like branches touching at a single point (Figure 1a, left panel). In sufficiently large applied B, the charges' cyclotron orbits coalesce to form discrete LLs, with energy given by[20,41−43]

$$E_{M,N} = \pm\sqrt{2\hbar v_F^2 eB|N|} \quad \text{and}$$
$$E_{B,N} = \pm\frac{\hbar eB}{m^*}\sqrt{N(N-1)} \tag{1}$$

The lowest LL is 12-fold degenerate, giving rise to quantized plateaus at filling factors $\nu = n\hbar/Be$ = ...−10, −6, 6, 10, 14.... Here e is electron charge, n is the induced charge density, $\hbar$ is Planck's constant, $v_F \sim 10^6$ m/s the Fermi velocity, $m^* = \gamma_1/(\sqrt{2}v_F^2) \sim 0.02$−$0.04\ m_e$, m_e is the electron rest mass, $\gamma_1 \sim 0.3$ eV is the interlayer coupling, and N is an integer denoting the LL index. Figure 2a shows the standard LL "fan diagram" of the device, that is, G (color scale) as a function of V_{bg} (horizontal axis) and B (vertical axis). The QH plateaus appear as the colored bands that diverge from $B = 0$ and the charge neutrality point (CNP). The small apparent curvature in the fan diagram for small B arises from the smeared crossing between MLG-like and BLG-like bands, which will be discussed further below. From the fan diagram, the back gate's coupling efficiency is estimated to be $\alpha_{bg} \sim 3.8 \times 10^{10}$ cm^{-2}/V, which also agrees with that calculated from device geometry.

To accentuate the evolution of the QH plateaus with V_{bg} and B, we plot dG/dV_{bg} (V_{bg}, B) of the same data set in Figure 2b. The filling factor of each plateau, which appears as a white band, $\nu = n\hbar/Be = \alpha_{bg}V_{bg}h/Be$, is calculated from its slope in the V_{bg}−B plane and labeled in Figure 2b. The most prominent feature is the very strong $\nu = -2$ plateau in the hole-doped regime, which is resolved at B as small as 0.25 T. (Here we define hole-doped and electron-doped regime to have negative and positive filling factors, respectively.) Line traces $G(V_{bg})$ at several B values for $B < 4.2$ T are shown in Figure 2c. When replotted as a function of ν, the traces nearly collapse into a single curve with properly quantized plateaus at $\nu = -2$, 2, 6, and 10.

dx.doi.org/10.1021/nl4000757 | Nano Lett. XXXX, XXX, XXX−XXX

The appearance of robust $\nu = 6$ and 10 states agrees with eq 1 as well as prior reports.[30,33,35] On the other hand, our observation of the $\nu = 2$ and in particular the exceedingly robust $\nu = -2$ plateaus, is unexpected from eq 1. This can however be accounted for by the "2 + 1" model that takes remote hopping into account instead of MLG-like and BLG-like bands both touching at a single point, including next-nearest hopping parameters (γ_2 and γ_5) leads to bands that are individually gapped, with a relative vertical offset between the MLG-like and BLG-like bands, whose tops of valence bands are located at $-\gamma_2/2$ and $\gamma_2/2$, respectively (Figure 1a, right panel). Consequently, the LL spectrum of such a band structure is modified from eq 1 as follows: (i) since ABA stacked TLG obeys mirror symmetry but not inversion symmetry,[36] its valley degeneracy is not protected; the broken valley degeneracy of the lowest LL[36] manifests as $\nu = \pm 2$ plateaus, as observed experimentally; (ii) the spectrum is particle-hole asymmetric; and (iii) LLs originating from the MLG-like and BLG-like bands cross at energy $\sim\pm\gamma_2/2$.

All three features are observed in our experimental data. Apart from the robust $\nu = \pm 2$ plateaus, the particle-hole asymmetry is clearly reflected in the sequence of resolved plateaus; the $\nu = 6$ and 10 plateau is observed only in the electron doped regime and $\nu = -8$ is observed solely in the hole-doped regime. The dark blue feature at $V_{bg} \sim -5$ V, indicated by the dotted circle in Figure 2b, corresponds to the crossings between LLs that belong to the MLG and BLG-like spectra.[36] From the data, the crossings occur at $\sim -1.9 \times 10^{11}$ cm^{-2}, corresponding to ~ -8 meV. Thus our data suggest $\gamma_2 \sim -16$ meV in TLG, in reasonable agreement with the value from bulk graphite, -20 meV.[44]

Thus far the $\nu = -2$, 2, 6, and 10 plateaus are well accounted for by single particle tight binding calculations, using values of hopping parameters obtained from graphite. (The absence of the $\nu = -6$ state is an experimental surprise and currently not understood). At larger B, we also observe additional plateaus at $\nu = \pm 1$, ± 3, -4, and -5, which indicate almost complete lifting of spin, valley and orbital degeneracies in the lowest LL. The $\nu = 0$ plateau, although resolved, is $\sim 0.3\ e^2/\hbar$ at 18 T. This lack of true insulating behavior is likely due to the presence of small amount of residual impurities. Figure 2d plots $G(V_{bg})$ and $G(\nu)$ at $B = 4.5$, 6, 7, 8 and 10 T, respectively, showing satisfactory conductance quantization. The $\nu = \pm 1$ plateaus are resolved at B as low as 4.5 T and persists to 18 T (Figure 2e,f), the highest available field. These additional plateaus, particularly those at odd filling factors, cannot be accounted for by any tight binding model or simple breaking of layer symmetry due to the presence of an out-of-plane electric field. Instead, the plateaus' appearance at high B values in samples with high mobility ($\geq$10 000 cm^2/(V s)) strongly suggests symmetry breaking arising from electronic interactions. In fact, they can be qualitatively understood in terms of QH ferromagnetism and Hunds rule-like filling of the 12-fold degenerate lowest LL.[45] Within this model, the LLs between $\nu = -6$ and 6 are filled in the order of maximizing spin, chirality (BLG-like branch first), valley, and orbital indices. At large B, the $\nu = -5$, -4, -3, -2, 1, 2, and 3 states belong to the BLG-like branch, while the $\nu = -1$, 0, +4, and +5 states to the MLG-like branch.[43] (The $\nu = 4$ and $\nu = -2$ are marginal cases as they separates a series of bilayer-like LL's and a series of monolayer-like LL's. For instance, at $\nu = 4$, for positive energies the last $N = 0$ bilayer-like LL is filled or the first $N = 0$ MLG-like LL is empty.) As observed experimentally, all the BLG-like states are fully resolved, whereas only the $\nu = -1$ (and to some extent the $\nu = 0$) state in the SLG-like branches is observed.

We now focus on the QH states in the presence of both top and back gates. Sweeping both top and back gate voltages enables independent modulation of the electric field $E_\perp$ and total charge carrier density n in TLG, which has emerged as a critical tool to study the broken symmetry states in bilayer graphene.[14−16] For ABA-stacked TLG, $E_\perp$ breaks its mirror reflection symmetry and is expected to give rise to Landau crossings, otherwise unresolved plateaus or the stabilization of existing plateau with finite $E_\perp$.[46,47]

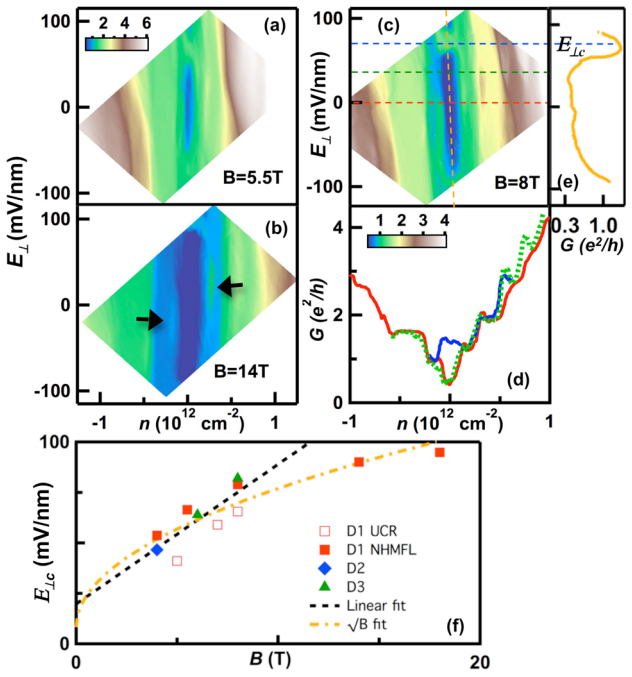

Figure 3. (a−c) $G(n, E_\perp)$ in units of $e^2/\hbar$ at $B = 5.5$, 14 and 8 T. (a,b) These panels have the same color scale, and color scale of (c) is shown in panel d. The arrows in (b) indicate the asymmetry in $E_\perp$ in electron- and hole-doped regimes. (d) $G(n)$ along the horizontal lines in (c) at $E_\perp = 0$ (red), 43 (green dotted line), and 73 mV/nm (blue), respectively. (e) $G(E_\perp)$ along the vertical line in (c) at $n = 0$. (f) $E_{\perp c}(B)$ from three different devices. The black and orange lines correspond to linear and $B^{1/2}$ fits, respectively.

In Figure 3a−c, G (color scale) is plotted as a function of $E_\perp$ (vertical axis) and n (horizontal axis) at $B = 5.5$, 8, and 14 T, respectively. Here n and $E_\perp$ are calculated by

$$n = \alpha_{bg}(V_{bg} - V_{bg}^D) + \alpha_{tg}(V_{tg} - V_{tg}^D) \equiv n_{bg} + n_{tg}$$

$$E_\perp = \frac{(n_{bg} - n_{tg})e}{2\varepsilon_0}$$

where V^D is the Dirac point, α is the coupling efficiency, ε_0 is the permittivity of vacuum, and the subscripts indicate back gate and top gate, respectively. The vertical color bands correspond to the conductance plateaus at different filling factors. Figure 3d plots $G(n)$ at $B = 8$ T and $E_\perp = 0$, 43, and 73 mV/nm, respectively. At $E_\perp = 0$, plateaus $\nu = 0$, 1, 2, and 3 are observed. At $E_\perp = 43$ mV/nm, the first three plateaus remain

dx.doi.org/10.1021/nl4000757 | Nano Lett. XXXX, XXX, XXX−XXX

relatively unchanged, whereas the $\nu = 3$ plateau is better resolved, and the $\nu = 4$ plateau emerges. Thus, our data suggest that layer polarization is an important component in the $\nu = 3$ and 4 states.

In contrast to the electron-doped regimes, the hole plateaus in Figure 3d, though resolved, are not perfectly quantized: conductance at filling factor $\nu = -1$, -2, and -4 are ~1, 1.7, and 2.8, respectively. This arises from the slightly lower hole mobility (25% lower than electrons) in this particular device, which may result from the presence of scatterers that preferentially scatter holes.

Another striking feature in these $G(n, E_\perp)$ plots is the dependence of the $\nu = 0$ plateau on $E_\perp$; it abruptly increases from 0.3 to ~1 $e^2/\hbar$ at a critical $E_{\perp c}$ value and decreases to 0.3 again for a larger $E_\perp$ (Figure 3e). The $G(n)$ trace at $E_{\perp c}$ is characterized by the absence of the $\nu = 0$ plateau (Figure 3d, blue line). Taken together, our data suggest a transition from spin-ordered to layer-polarized states driven by B and $E_\perp$, respectively, and is highly reminiscent of that in BLG.[14−16]

To further investigate the transition between the LLs, we examine the dependence of $E_{\perp c}$ on B. In BLG, $E_{\perp c}$ is linearly dependent on B with a slope ~13 mV/nm/T and extrapolates to a finite value ~12 mV/nm at $B = 0$.[14−16] Figure 3f plots $E_{\perp c}$ versus B for three different devices (device D1 was measured at two separate locations). For $B < 8$T, within the scatter in the data $E_{\perp c}$ is approximately linear in B, with a best-fit equation $E_{\perp c}$ (mV/nm) = 19.7 + 6.9B. Interestingly, when B is extended to 18 T, the data points are no longer linear; instead, they can be adequately fitted to the equation $E_{\perp c}$ (mV/nm) = 8.3 + 21.7$B^{1/2}$, suggesting that Coulomb interactions play an essential role at higher B.[48] There is little theoretical work on LL transitions in ABA-stacked TLG in the presence of electric and magnetic fields, and this phenomenon warrants further experimental and theoretical investigation.

Finally, we focus on a peculiar feature of the conductance in the presence of $E_\perp$ and B. Figure 4 plots $G(E_\perp,n)$ at $B = 7$ T. At

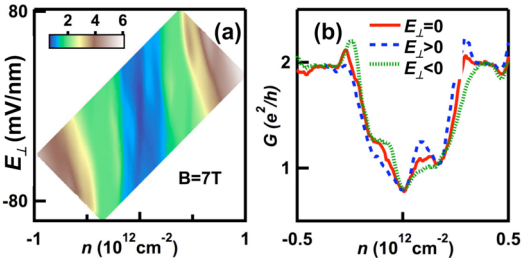

Figure 4. (a). $G(n, E_\perp)$ at $B = 7$ T in units of $e^2/\hbar$. (b). $G(n)$ at $E_\perp = 0$ (red solid line), -17 (green dotted line), and 13.6 mV/nm (blue dashed line).

finite $E_\perp$, the $G(n)$ traces are asymmetric with respect to electrons and holes. Interestingly, such asymmetry depends on the direction of the applied $E_\perp$, and reverses upon reversal of the sign of $E_\perp$. In Figure 4a, this asymmetry can be seen as the asymmetric appearance of the bright blue band to the right (left) of the charge neutrality point for positive (negative) $E_\perp$. A similar asymmetry can be seen in Figure 3a, as indicated by the arrows. Figure 4b plots the $G(n)$ curves at $E_\perp = 0$, -17, and 13.6 mV/nm, respectively. The $\nu = -1$ plateau was only resolved for $E_\perp < 0$, whereas the $\nu = 1$ state was better resolved for $E_\perp > 0$. Thus, $E_\perp$ appears to selectively break the symmetry of LLs of the electron- or hole-doped regimes, depending on its polarity. We currently do not have an explanation for this phenomenon. It may be related to the particle-hole asymmetry in few layer graphene's band structure,[49] or to more intriguing phenomena such as spin−orbit interactions or magneto-electric effects.[50,51] Further experimental investigation will be necessary to fully elucidate its origin.

In conclusion, using dual-gated high mobility samples, we observe several intriguing phenomena related to the broken symmetry QH states in ABA-stacked TLG, including almost complete lifting of the spin, valley, and orbital degeneracies of the lowest LL, stabilization of some of these states by $E_\perp$, transition between LLs driven by $E_\perp$ and B, and a particle-hole asymmetry that depends on the polarity of $E_\perp$. Our study demonstrates the rich interaction physics in ABA TLG in the $E_\perp$−B−n phase space. A number of unresolved questions, such as the dependence of $E_{\perp c}$ on B at large field and dependence of the electron−hole asymmetry on $E_\perp$, await further studies.

AUTHOR INFORMATION

Corresponding Author

*E-mail: lau@physics.ucr.edu.

Notes

The authors declare no competing financial interest.

ACKNOWLEDGMENTS

We thank Yafis Barlas for helpful discussions. This work was supported in part by NSF CAREER DMR/0748910, NSF/1106358 and the FAME Center. F.Z. was supported by DARPA SPAWAR N66001-11-1-4110. Part of this work was performed at NHMFL that is supported by NSF/DMR-0654118, the State of Florida, and DOE. This material is partly based on research sponsored by DARPA/DMEA H94003-10-2-1003. U.S. Government is authorized to reproduce and distribute reprints for Government purposes, notwithstanding any copyright notation thereon.

REFERENCES

(1) Novoselov, K. S.; Geim, A. K.; Morozov, S. V.; Jiang, D.; Zhang, Y.; Dubonos, S. V.; Grigorieva, I. V.; Firsov, A. A. *Science* **2004**, *306*, 666−669.

(2) Fuhrer, M. S.; Lau, C. N.; MacDonald, A. H. *MRS Bull.* **2010**, *35*, 289−295.

(3) Lau, C. N.; Bao, W.; Velasco, J., Jr. *Mater. Today* **2012**, *15*, 238−245.

(4) Du, X.; Skachko, I.; Duerr, F.; Luican, A.; Andrei, E. Y. *Nature* **2009**, *462*, 192−195.

(5) Bolotin, K. I.; Ghahari, F.; Shulman, M. D.; Stormer, H. L.; Kim, P. *Nature* **2009**, *462*, 196−199.

(6) Dean, C. R.; Young, A. F.; Cadden-Zimansky, P.; Wang, L.; Ren, H.; Watanabe, K.; Taniguchi, T.; Kim, P.; Hone, J.; Shepard, K. L. *Nat. Phys.* **2011**, *7*, 693−696.

(7) Young, A. F.; Dean, C. R.; Wang, L.; Ren, H.; Cadden-Zimansky, P.; Watanabe, K.; Taniguchi, T.; Hone, J.; Shepard, K. L.; Kim, P. *Nat. Phys.* **2012**, *8*, 550−556.

(8) Checkelsky, J. G.; Li, L.; Ong, N. P. *Phys. Rev. Lett.* **2008**, *100*, 206801.

(9) Checkelsky, J. G.; Li, L.; Ong, N. P. *Phys. Rev. B* **2009**, *79*, 115434.

(10) Zhao, Y.; Cadden-Zimansky, P.; Jiang, Z.; Kim, P. *Phys. Rev. Lett.* **2010**, *104*, 066801.

(11) Feldman, B. E.; Martin, J.; Yacoby, A. *Nat. Phys.* **2009**, *5*, 889−893.

(12) Veligura, A.; van Elferen, H. J.; Tombros, N.; Maan, J. C.; Zeitler, U.; van Wees, B. J. *Phys. Rev. B* **2012**, *85*, 155412.

(13) Freitag, F.; Trbovic, J.; Weiss, M.; Schonenberger, C. *Phys. Rev. Lett.* **2012**, *108*, 076602.
(14) Weitz, R. T.; Allen, M. T.; Feldman, B. E.; Martin, J.; Yacoby, A. *Science* **2010**, *330*, 812−816.
(15) Velasco, J.; Jing, L.; Bao, W.; Lee, Y.; Kratz, P.; Aji, V.; Bockrath, M.; Lau, C. N.; Varma, C.; Stillwell, R.; Smirnov, D.; Zhang, F.; Jung, J.; MacDonald, A. H. *Nat. Nanotechnol.* **2012**, *7*, 156.
(16) Maher, P.; Dean, C. R.; Young, A. F.; Taniguchi, T.; Watanabe, K.; Shepard, K. L.; Hone, J.; Kim, P. *Nat. Phys.* **2013**, *9*, 1−5.
(17) Bao, W.; Velasco, J.; Zhang, F.; Jing, L.; Standley, B.; Smirnov, D.; Bockrath, M.; MacDonald, A. H.; Lau, C. N. *Proc. Natl. Acad. Sci. U.S.A.* **2012**, *109*, 10802−10805.
(18) Zhang, L.; Zhang, Y.; Camacho, J.; Khodas, M.; Zaliznyak, I. A. *Nat. Phys* **2011**, *7*, 953−957.
(19) Bao, W.; Jing, L.; Lee, Y.; Velasco, J., Jr.; Kratz, P.; Tran, D.; Standley, B.; Aykol, M.; Cronin, S. B.; Smirnov, D.; Koshino, M.; McCann, E.; Bockrath, M.; Lau, C. N. *Nat. Phys.* **2011**, *7*, 948−952.
(20) Guinea, F.; Castro Neto, A. H.; Peres, N. M. R. *Phys. Rev. B* **2006**, *73*, 245426.
(21) Aoki, M.; Amawashi, H. *Solid State Commun.* **2007**, *142*, 123−127.
(22) Koshino, M.; McCann, E. *Phys. Rev. B* **2009**, *79*, 125443.
(23) Zhang, F.; Sahu, B.; Min, H. K.; MacDonald, A. H. *Phys. Rev. B* **2010**, *82*, 035409.
(24) Manes, J. L.; Guinea, F.; Vozmediano, M. A. H. *Phys. Rev. B* **2007**, *75*, 155424.
(25) Partoens, B.; Peeters, F. M. *Phys. Rev. B* **2006**, *74*, 075404.
(26) Latil, S.; Henrard, L. *Phys. Rev. Lett.* **2006**, *97*, 036803.
(27) Koshino, M. *Phys. Rev. B* **2010**, *81*, 125304.
(28) Yuan, S.; Roldaacuten, R.; Katsnelson, M. I. *Phys. Rev. B* **2011**, *84*, 125455.
(29) Bao, W.; Zhao, Z.; Zhang, H.; Liu, G.; Kratz, P.; Jing, L.; Velasco, J.; Smirnov, D.; Lau, C. *Phys. Rev. Lett.* **2010**, *105*, 246601.
(30) Taychatanapat, T.; Watanabe, K.; Taniguchi, T.; Jarillo-Herrero, P. *Nat. Phys.* **2011**, *7*, 621.
(31) Lui, C. H.; Li, Z.; Mak, K. F.; Cappelluti, E.; Heinz, T. F. *Nat. Phys.* **2011**, *7*, 944.
(32) Craciun, M. F.; Russo, S.; Yamamoto, M.; Oostinga, J. B.; Morpurgo, A. F.; Thrucha, S. *Nat Nanotechnol* **2009**, *4*, 383−388.
(33) Henriksen, E. A.; Nandi, D.; Eisenstein, J. P. *Phys. Rev. X* **2012**, *2*, 011004.
(34) Jhang, S. H.; Craciun, M. F.; Schmidmeier, S.; Tokumitsu, S.; Russo, S.; Yamamoto, M.; Skourski, Y.; Wosnitza, J.; Tarucha, S.; Eroms, J.; Strunk, C. *Phys. Rev. B* **2011**, *84*, 161408.
(35) Khodkov, T.; Withers, F.; Hudson, D. C.; Craciun, M. F.; Russo, S. *Appl. Phys. Lett.* **2012**, *100*, 013114.
(36) Koshino, M.; McCann, E. *Phys. Rev. B* **2011**, *83*, 165443.
(37) Ferrari, A. C.; Meyer, J. C.; Scardaci, V.; Casiraghi, C.; Lazzeri, M.; Mauri, F.; Piscanec, S.; Jiang, D.; Novoselov, K. S.; Roth, S.; Geim, A. K. *Phys. Rev. Lett.* **2006**, *97*, 187401.
(38) Liu, G.; Velasco, J.; Bao, W.; Lau, C. N. *Appl. Phys. Lett.* **2008**, *92*, 203103.
(39) Velasco, J., Jr; Liu, G.; Bao, W.; Ning Lau, C. *New J. Phys.* **2009**, *11*, 095008.
(40) Lui, C. H.; Li, Z.; Chen, Z.; Klimov, P. V.; Brus, L. E.; Heinz, T. F. *Nano Lett.* **2011**, *11*, 164−169.
(41) McClure, J. W. *Phys. Rev.* **1956**, *104*, 666−671.
(42) McCann, E.; Fal'ko, V. I. *Phys. Rev. Lett.* **2006**, *96*, 086805.
(43) Ezawa, M. *J. Phys. Soc. Jpn.* **2007**, *76*, 094701.
(44) Dresselhaus, M. S.; Dresselhaus, G. *Adv. Phys.* **2002**, *51*, 1−186.
(45) Zhang, F.; Tilahun, D.; MacDonald, A. H. *Phys. Rev. B* **2012**, *85*, 165139.
(46) Morimoto, T.; Koshino, M. preprint 2013, arXiv:1211.7189v2, (accessed Mar 22, 2013).
(47) Serbyn, M.; Abanin, D. A. preprint 2013, arXiv:1212.6251v2, (accessed Mar 22, 2013).
(48) Herbut, I.; Roy, B. *Phys. Rev. B* **2008**, *77*, 245438.
(49) Zhang, L. M.; Fogler, M. M.; Arovas, D. P. *Phys. Rev. B* **2011**, *84*, 075451.
(50) Zhu, L.; Aji, V.; Varma, C. M. *Phys. Rev. B* **2012**, *87*, 035427.
(51) Winkler, R.; Zuelicke, U. preprint 2012, arxiv:1206.4761, (accessed July 7, 2012).